Effects of Ag Doping on Texture and Magnetic Properties of Directionally Solidified Fe-17%Ga Alloys

Zhiyong Dai [1], Chao Zhou [1,*], Qizhong Zhao [1], Kaiyan Cao [1], Zhengming Zhang [2], Dunhui Wang [2], Dezhen Xue [3], Adil Murtaza [1], Yin Zhang [1], Fanghua Tian [1], Wenliang Zuo [1], Yoshitaka Matsushita [4], Sen Yang [1,3,*], Xiaoping Song [1]

[1] *MOE Key Laboratory for Nonequilibrium Synthesis and Modulation of Condensed Matter, School of Physics, Xi'an Jiaotong University, Xi'an 710049, China*

[2] *Division of Microelectronic Materials and Devices, Hangzhou Dianzi University, Hangzhou 310018, China*

[3] *State Key Laboratory for Mechanical Behavior of Materials, School of Materials Science and Engineering, Xi'an Jiaotong University, Xi'an 710049, China*

[4] *National Institute for Materials Science, Tsukuba, Ibaraki 305-0047, Japan*

Abstract

FeGa-based alloys are potential candidates in magneto-mechanical transversion applications. It has been demonstrated that doping with certain elements results in the increase of λ_{100} and modification of the texture, both of which effectively enhance the magnetostriction of FeGa. However, the contribution of each factor is difficult to distinguish because of lacking an effective physical model. In this work, based on independence of saturation magnetostriction (λ_s) on magnetic domain distribution, a paradigm that combines the orientation distribution function and magnetostriction tensor of single crystals is employed to quantify effects of texture on magnetostriction and predict λ_{100}. Then this paradigm is applied to Ag-doped FeGa and the results reveal that the enhancement of λ_{100} plays a more crucial role in the enhancement of λ_s after Ag doping. Our work clarifies the contribution to magnetostriction enhancement from texture and λ_{100} in element-doped FeGa alloys, and may help develop more high-performance FeGa alloys.

Authors to whom correspondence should be addressed: chao.zhou@xjtu.edu.cn; yang.sen@xjtu.edu.cn.

Magnetostrictive materials have wide applications in magnetic sensors, actuators, transformers, and energy harvesters. Compared to ferromagnetic martensite alloys [1] and Laves phase rare earth-transition metal compounds [2], FeGa-based alloys exhibit comparatively lower magnetostriction. Many efforts have been devoted, e.g., doping with a trace amount of rare earth elements proves to have a significant effect on magnetostriction of FeGa alloys. By doping with 0.2% Dy in Fe-17% Ga, magnetostriction increases from 70 ppm to 150 ppm at 1000 Oe [3]. Besides, doping with Tb [4], Y [5], and Ce [6] shows similar effects.

The magnetostriction enhancement after doping with certain elements is attributed to the increase of tetragonal magnetostrictive constant (λ_{100}), e.g., Tb [7], or modification of the preferred orientation of crystals in polycrystalline aggregates (i.e., texture) [8], e.g., Tb [4], Er [9], Pt [10], Sm [6]. Because of lacking an effective physical model, the contribution of each factor is difficult to distinguish, making it impossible to systematize theoretical research and engineering practice.

Here, we propose a paradigm to distinguish the contribution of each factor. For single crystals, $\lambda_{\parallel}$ and $\lambda_{\perp}$ (measured in a direction when the applied field is parallel and vertical to measurement direction, respectively) are dependent on initial magnetic domain distribution, but saturation magnetostriction λ_s ($= \lambda_{\parallel} - \lambda_{\perp}$) is not and remains constant [11]. For polycrystals, λ_s is also independent of initial domain distribution [12]. Thus, λ_s of a particular distribution of magnetic domains is equal to that of ideal demagnetization, which only depends on texture. Orientation distribution function (ODF) is combined with the magnetostriction tensor of single crystals, by which effects of texture on magnetostriction can be quantified. Rare earth element-rich phases are easy to precipitate from rare earth element-doped FeGa alloy [3-6, 9]. Approximately, magnetostriction of FeGa alloy which is composed of different phases, obeys a rule of mixture relationship [13]. So, apart from A2 phase (alpha iron-based disorder phase), characterization of rare earth element-rich phases (ODFs of textures and magnetostriction tensors of single crystals) needs to be taken into consideration, which makes computation complicated. For simplicity, we choose a non-magnetic element as an example, which will only include A2 phase for consideration and omit possible element-rich precipitates for their negligible volume and magnetostriction. By DFT calculation, Ag and Cu are potential elements that can effectively enhance λ_{100} [14]. So, in the present study, Ag is chosen to be the doping element as an example, to quantify the effects of doping on λ_{100} and texture in FeGa alloy. Besides, directional solidification with a high withdrawal

speed is used to decrease precipitation of Ag and obtain good textures [15]. Microstructure and magnetic properties of $Fe_{83}Ga_{17}$ and $(Fe_{0.83}Ga_{0.17})_{99.8}Ag_{0.2}$ were investigated, while distribution of magnetic domains was also studied by magnetic domain patterns.

The $(Fe_{0.83}Ga_{0.17})_{100-x}Ag_x$ polycrystalline samples (x represents the atomic percentages; x = 0, 0.2) were prepared by arc-melting techniques under argon atmosphere, using high purity metals of Fe (99.95%), Ga (99.99%) and Pt (99.99%). To ensure compositional homogeneity, each sample was melted four times [16]. The directionally solidified samples were prepared at 1650℃ with the withdrawal rate of 1800 mm/h. The samples were cut by the electric-spark method along the directional solidification direction and the fin al size of samples for tests is 8 mm × 8 mm × 1.5 mm. The macrostructure was investigated by optical microscopy and columnar grains were confirmed to be arranged parallelly to growth direction in Fig. S1. The X-ray diffraction (XRD) patterns were measured by using a Bruker D8 ADVANCE Diffractometer (Cu–Kα, λ = 1.5406 Å) at room temperature. For texture analysis, pole figures from the (110), (200), and (211) reflections were collected at room temperature. To cover the pole sphere, 2θ = 30°~90°, Ψ = 0°~75° and φ = 0 to 360˚ in 5˚ increments. Iron alpha (A2 phase) is expected to be contained. The raw XRD data were processed using Bruker DIFFRAC.TEXTURE software (the harmonic series expansion method, thirty-four series rank L = 34, orthotropic sample symmetry). Then the data were analyzed by the MATLAB toolbox MTEX to obtain the orientation distribution function (ODF) plots [17]. The magnetic characterization was carried out on the superconducting quantum interference device - vibrating sample magnetometer (MPMS-SQUID VSM-094) at 300 K. The magnetostriction was tested at 300 K, with standard strain gauges which were pasted on samples and parallel to rod growth direction. Longitudinal and transverse measurements were taken by applying the magnetic field parallel and transverse to the strain gauges respectively, while keeping the magnetic field in the slab plane. Strain gauges are BX120-1AA (120 Ω resistance, sensitivity coefficient 2.08 ± 0.01), produced by Ningbo YaoNan Electromechanical Equipment Co. (Ningbo, China). The magnetic domain was observed by magnetic force microscopy (MFM, Bruker Innova) at room temperature and pictures were exported by NanoScope Analysis. The MFM samples were firstly polished by silicon carbide sandpapers and at final treatment by electrolytic polishing.

Fig.1(a) presents XRD patterns of directionally solidified $(Fe_{0.83}Ga_{0.17})_{100-x}Ag_x$ (x = 0, 0.2) polycrystalline samples. Only A2 phase is detected for both samples, and peaks from phases

related to Ag are not manifested, like Fe-based ribbons doped with 1 at.% Ag [18]. The scheme of the relationship between specimen coordinate system (the rolling direction (RD), the transverse direction (TD), and the rolling plane normal direction (ND)) and crystal growth direction is illustrated in Fig.1 (b). Fig. 1(c) and 1(d) show ODF plots of $(Fe_{0.83}Ga_{0.17})_{100-x}Ag_x$ (x=0, 0.2) samples from XRD texture analysis. The orthotropic sample symmetry was imposed on the calculation, mainly due to the symmetry of the magnetostriction tests along three directions, i.e. RD, TD, and ND. The ODF plots demonstrate that, by doping with Ag, sample texture changes from near Goss texture {011}<100> to near Cube texture {001}<100>. Since the "cube texture", {001}<100>, is better than Goss texture {011}<100> for enhancing magnetostriction [19], it is expected that the formation of a preferred texture presented by ODF plots enhances magnetostrictive properties [20]. In consideration of the increase of intensity in ODF plots far from Goss texture and Cube texture, the total effect of texture change by Ag doping still needs to be studied.

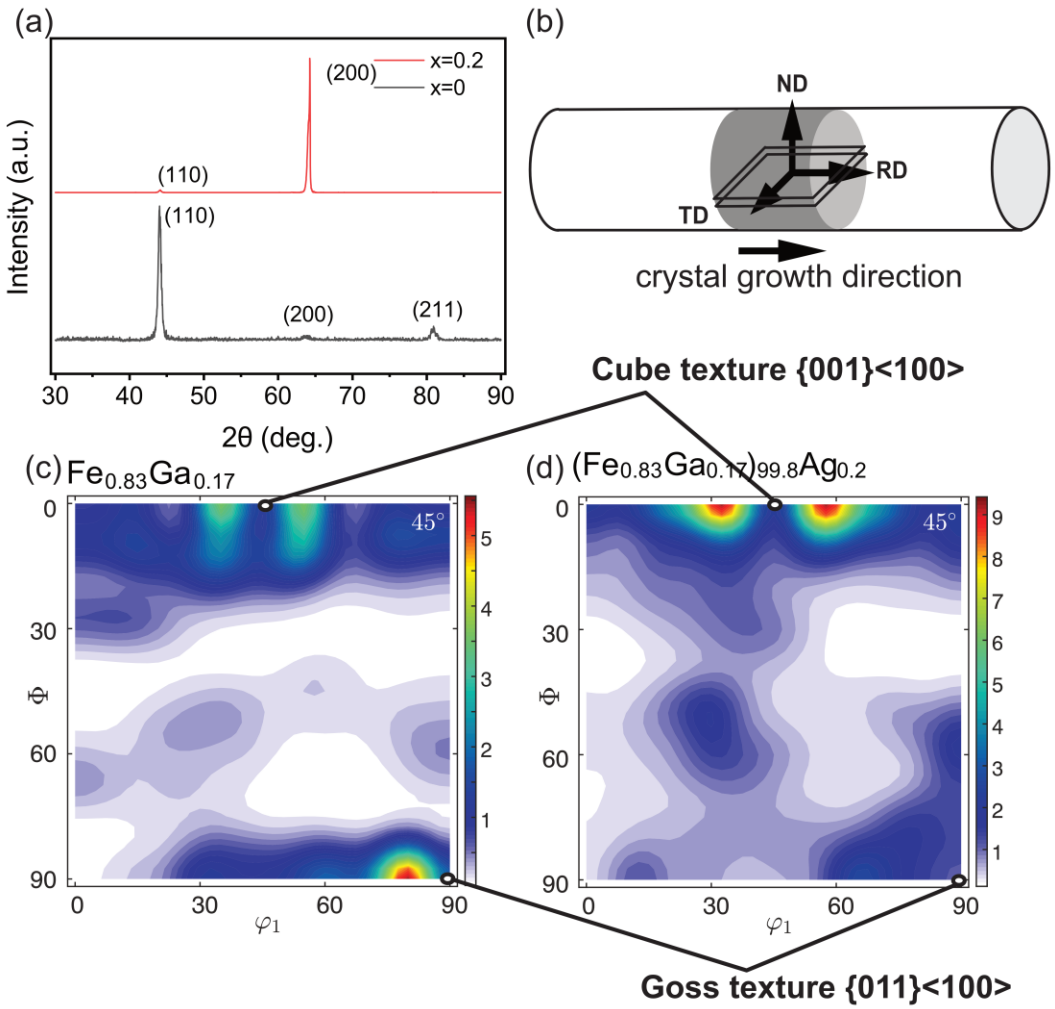

Fig. 1 (a) X-ray diffraction patterns of directionally solidified $(Fe_{0.83}Ga_{0.17})_{100-x}Ag_x$ (x = 0, 0.2) samples at room temperature. (b) the scheme of the relationship between specimen coordinate system (RD, TD, and ND) and crystal growth direction. (c) ODF plot (φ_2 = 45°) of directionally solidified $Fe_{0.83}Ga_{0.17}$ sample at room temperature. (d) ODF plot (φ_2 = 45°) of directionally solidified $(Fe_{0.83}Ga_{0.17})_{99.8}Ag_{0.2}$ sample at room temperature.

Magnetostriction curves of two samples are shown in Fig. 2(a) and 2(b). $\lambda_{\parallel}$ is measured along RD with the magnetic field along RD, while $\lambda_{\perp}$ is measured along RD with the magnetic field along TD. For $Fe_{0.83}Ga_{0.17}$, magnetostrictions at H = 3000 Oe (magnetization is saturated and the direction is parallel to the applied magnetic field, which will be shown in the following Fig. 3) are $\lambda_{\parallel}$ = 120 ppm, $\lambda_{\perp}$ = -52 ppm and λ_s = 172 ppm. For $(Fe_{0.83}Ga_{0.17})_{99.8}Ag_{0.2}$, magnetostrictions at H = 3000 Oe are $\lambda_{\parallel}$ = 100 ppm, $\lambda_{\perp}$ = -130 ppm and λ_s = 230 ppm. By doping with Ag, saturation magnetostriction λ_s increases.

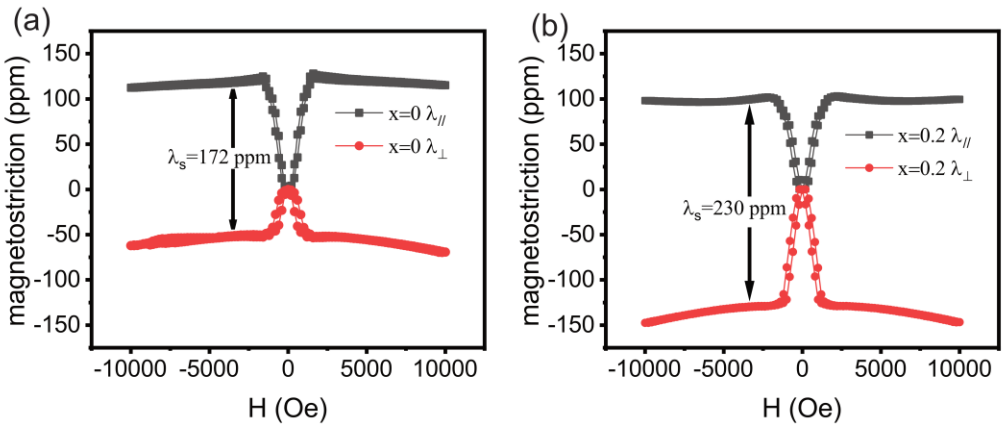

Fig. 2 Magnetostrictions of directionally solidified $(Fe_{0.83}Ga_{0.17})_{100-x}Ag_x$ samples at 300 K: (a) x = 0, (b) x = 0.2.

Anisotropy of many properties can be evaluated from the knowledge of the single-crystal tensors and ODF of crystals in polycrystals [21]. Magnetostriction in polycrystalline textured materials can be described by a 4-rank tensor $\lambda_{ijkl}(g)$ defined in the specimen reference frame [22]. Here, g = (φ1, Φ, φ2), describing the crystallographic orientation. ODF, which will be denoted by f(g), represents the normalized probability density that quantifies the occurrence of the crystallographic orientation, g. Then the Voigt average of a specimen is [22],

$$\bar{\lambda}_{ijkl} = \oint \lambda_{ijkl}(g) f(g) dg \quad (1)$$

Furthermore, $\lambda_{ijkl}(g)$ can be expressed by the single crystal constants λ^0_{mnop} [23],

$$\lambda_{ijkl}(g) = \lambda^0_{mnop} \cdot g_{im} \cdot g_{jn} \cdot g_{ko} \cdot g_{lp} \quad (2)$$

and g_{ij} is rotation. Hence, Eq. (1) can be written as [23],

$$\overline{\lambda_{ijkl}} = \lambda^0_{mnop} \cdot \overline{T^{mnop}_{ijkl}} \quad (3)$$

where the quantities $\bar{T}$ depend only on the texture [23],

$$\overline{T^{mnop}_{ijkl}} = \oint g_{im} \cdot g_{jn} \cdot g_{ko} \cdot g_{lp} \cdot f(g) \cdot dg \quad (4)$$

For a single cubic crystal at the ideal demagnetized state, the magnetostriction tensor matrix is [24],

$$\lambda^0_{mnop} = \begin{vmatrix} \lambda_{100} & -\frac{1}{2}\lambda_{100} & -\frac{1}{2}\lambda_{100} & 0 & 0 & 0 \\ -\frac{1}{2}\lambda_{100} & \lambda_{100} & -\frac{1}{2}\lambda_{100} & 0 & 0 & 0 \\ -\frac{1}{2}\lambda_{100} & -\frac{1}{2}\lambda_{100} & \lambda_{100} & 0 & 0 & 0 \\ 0 & 0 & 0 & \frac{3}{4}\lambda_{111} & 0 & 0 \\ 0 & 0 & 0 & 0 & \frac{3}{4}\lambda_{111} & 0 \\ 0 & 0 & 0 & 0 & 0 & \frac{3}{4}\lambda_{111} \end{vmatrix} \quad (5)$$

So, we can predict magnetostriction of polycrystals grown by directional solidification at the ideal demagnetized state. For $Fe_{0.83}Ga_{0.17}$ alloy, λ_{100} = 200 ppm, λ_{111} = -11 ppm [25]. Calculated by the function *calcTensor* in MTEX [17, 21] (a Matlab toolbox) with ODF of $Fe_{0.83}Ga_{0.17}$ sample, $\lambda_{\parallel}$ = 127 ppm, and $\lambda_{\perp}$ = -51 ppm, which is consistent with the experimental results. The calculated saturation magnetostriction λ_s (= 178 ppm) is close to the experimental result of 172 ppm with a 3.5% difference. This means that the calculation is fairly successful for saturation magnetostriction λ_s, and the sample is close to the ideal demagnetized state. Thus, magnetostriction of samples behaves like the Voigt average of polycrystalline aggregates. It also has been reported that Fe-Ga films grown on glass display a strong Voigt-type elastic behavior [26]. The magnetostriction enhancement may originate from not only texture change induced by Ag doping, but also changes of λ_{100} and λ_{111}. To distinguish the effect of texture change on magnetostrictive properties, induced by Ag doping, λ_{100} and λ_{111} of $Fe_{0.83}Ga_{0.17}$ alloy are put into calculation with ODF of $(Fe_{0.83}Ga_{0.17})_{99.8}Ag_{0.2}$ sample. We obtain that $\lambda_{\parallel}$ = 100 ppm, $\lambda_{\perp}$ = -42 ppm, and λ_s = 142 ppm. Comparing two calculation results of λ_s (142 ppm is 79.8% of 178 ppm), it is concluded that the total effect of texture change induced by doping with 0.2% Ag actually deteriorates the magnetostrictive properties of FeGa alloy.

We can also try to get a prediction of λ_{100} from our experimental results. Actually, predictions of $\lambda_{\parallel}$ and $\lambda_{\perp}$ are $\overline{\lambda_{1111}}$ and $\overline{\lambda_{1122}}$. So,

$$\overline{\lambda_{1111}} - \overline{\lambda_{1122}} = \lambda_s \quad (6)$$

If components of 0 in magnetostriction tensor λ^0_{mnop} are changed into a negligible value, e.g., 0.1, magnetostriction tensor matrix has an inverse matrix now (using function *inv* in MTEX). We mark a guess of magnetostriction tensor (0 changed into 0.1) as $\lambda^0_{mnop}{}'$, and its inverse matrix as $\left(\lambda^0_{mnop}{}'\right)^{-1}$. We calculate magnetostriction tensor matrix of polycrystal by the function *calcTensor* in MTEX,

$$\overline{\lambda_{ijkl}}' = \lambda^0_{mnop}{}' \cdot \overline{T^{mnop}_{ijkl}} \quad (7)$$

Then we calculate in Matlab with the equation,

$$\left(\lambda^0_{mnop}{}'\right)^{-1} : \overline{\lambda_{ijkl}}' = \left(\lambda^0_{mnop}{}'\right)^{-1} : \left(\lambda^0_{mnop}{}' \cdot \overline{T^{mnop}_{ijkl}}\right) \quad (8)$$

where double dot is inner product between tensors defined by MTEX.

We evaluate the equation symbolically,

$$\lambda^0_{mnop} : \left(\left(\lambda^0_{mnop}{}'\right)^{-1} : \overline{\lambda_{ijkl}}'\right) = \lambda^0_{mnop} : \left(\left(\lambda^0_{mnop}{}'\right)^{-1} : \left(\lambda^0_{mnop}{}' \cdot \overline{T^{mnop}_{ijkl}}\right)\right) \quad (9)$$

Then we get two equations which include three unknown parameters, i.e., $\overline{\lambda_{1111}}$, $\overline{\lambda_{1122}}$, and λ_{100} (prediction). Combining these two equations with Eq. (6), we can get values of $\overline{\lambda_{1111}}$, $\overline{\lambda_{1122}}$ and λ_{100} (prediction). Using the above steps, we get values of $\overline{\lambda_{1111}}$, $\overline{\lambda_{1122}}$ and λ_{100} (prediction) of $Fe_{0.83}Ga_{0.17}$ and $(Fe_{0.83}Ga_{0.17})_{99.8}Ag_{0.2}$ alloys, which are summarized in Table 1. From Table 1, the prediction of λ_{100} of $Fe_{0.83}Ga_{0.17}$ is close to the experimental value with a 3.5% difference. The predictions of $\lambda_{\parallel}$ and $\lambda_{\perp}$ of $(Fe_{0.83}Ga_{0.17})_{99.8}Ag_{0.2}$ are quite different from experimental values. This demonstrates that the initial demagnetized state is far from ideal. The prediction of λ_{100} of $(Fe_{0.83}Ga_{0.17})_{99.8}Ag_{0.2}$ is 325 ppm, which means a huge improvement (62.5%) from 200 ppm of $Fe_{0.83}Ga_{0.17}$ alloy. From the analysis of the total effect of texture change and λ_{100}, it can be concluded that the main contribution to enhancement of saturation magnetostriction λ_s comes from the enhancement of λ_{100} by doping with Ag. In Fig.1(a), in comparison with $Fe_{0.83}Ga_{0.17}$ sample, a clear asymmetry or splitting is shown in (200) peak of $(Fe_{0.83}Ga_{0.17})_{99.8}Ag_{0.2}$ sample. This peak splitting originates from A2 tetragonal distortion, and was also reported by Yangkun He et al. in $Fe_{0.83}Ga_{0.17}$ ribbons [27] and by Yijun Chen et al. in directionally solidified $(Fe_{0.81}Ga_{0.19})_{99.9}Tb_{0.1}$ crystals [28]. Symmetry lowering upon ferromagnetic transition is a general effect for all cubic ferromagnets [29], and symmetry in the calculations should be set as that before lowering. $D0_3$ phase is excluded, because no evidence of any $D0_3$ superlattice reflections is observed [30]. The modified-$D0_3$ nanoinclusions [27] are omitted because of their extremely low volume fraction and complexity of distinguishing (due to similar atom scattering factors of Fe and Ga atoms). So, the percentage of the tetragonal A2 phase in $(Fe_{0.83}Ga_{0.17})_{99.8}Ag_{0.2}$ sample is nearly 100%, as shown by the XRD data. The XRD data of $(Fe_{0.83}Ga_{0.17})_{99.8}Ag_{0.2}$ sample were analyzed by Rietveld refinement in Supplementary Fig. S2. A2 phase is transformed into a body-centered tetragonal lattice A_a phase (space group: I 4/m m m, 139) to obtain a and c values. For $(Fe_{0.83}Ga_{0.17})_{99.8}Ag_{0.2}$ sample, they are 2.89711 Å and 2.90719 Å, respectively. Thus, the

tetragonality, (c-a)/c = 0.003479. By doping with Ag, the tetragonality increases and is manifested in the XRD data.

Table 1 Comparison between experimental values and predictions for $\lambda_{\parallel}$, $\lambda_{\perp}$ and λ_{100} in $Fe_{0.83}Ga_{0.17}$ and $(Fe_{0.83}Ga_{0.17})_{99.8}Ag_{0.2}$ alloys

	$\lambda_{\parallel}$ (experimental)	$\lambda_{\parallel}$ (prediction)	$\lambda_{\perp}$ (experimental)	$\lambda_{\perp}$ (prediction)	λ_{100} (experimental)	λ_{100} (prediction)
$Fe_{0.83}Ga_{0.17}$	120	122	-52	-50	200 [25, 31]	193
$(Fe_{0.83}Ga_{0.17})_{99.8}Ag_{0.2}$	100	162	-130	-68	No data	325

Fig. 3 presents magnetization hysteresis loops of directionally solidified $(Fe_{0.83}Ga_{0.17})_{100-x}Ag_x$ (x = 0, 0.2) samples. From these loops, we can get saturation magnetization of $Fe_{0.83}Ga_{0.17}$, 182.4 emu/g, and $(Fe_{0.83}Ga_{0.17})_{99.8}Ag_{0.2}$, 190.4 emu/g. The saturation magnetization of $Fe_{0.83}Ga_{0.17}$ is in good agreement with that result, 184.76 emu/g reported by Lijuan Zhao et.al [32]. By doping with Ag, saturation magnetization increases. The increase of saturation magnetization may be due to lattice expansion, like doping with Pt [10], and Tb [33]. For $Fe_{0.83}Ga_{0.17}$ alloy, first order magnetocrystalline anisotropy constant, K_1 = 35 kJ/m^3 [34], and as-grown stress-induced anisotropy K_u of 1~10 kJ/m^3 [35]. So, quality factor $Q = K/K_d = K/(0.5\mu M_s^2) \ll 1$, where K is anisotropy energy and K_d is stray field energy [36, 37]. This results in in-plane domain patterns that minimize stray fields at the expense of anisotropy energy [38]. In this case, denser domain walls form in the surface zone and increase coercivity which is dominated by domain wall pinning in textured soft magnetic materials [37]. However, since volume of surface zone is small compared to bulk material, the increase in the coercive field is trivial. The inset in Fig. 3 plots the coercive fields and remnant magnetizations, which increase after doping with 0.2% Ag.

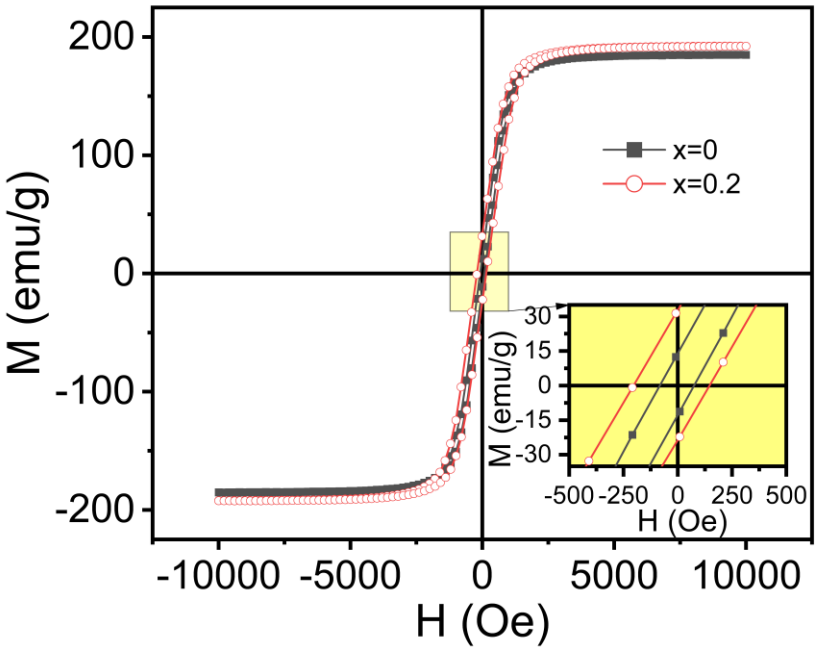

Fig. 3 Magnetization hysteresis loops of directionally solidified $(Fe_{0.83}Ga_{0.17})_{100-x}Ag_x$ (x = 0, 0.2) samples at 300 K. The inset plots the coercive fields and remnant magnetizations.

Fig. 4 (a) and 4(b) demonstrate magnetic domain patterns of directionally solidified $Fe_{0.83}Ga_{0.17}$ and $(Fe_{0.83}Ga_{0.17})_{99.8}Ag_{0.2}$ samples in the slab plane by MFM, respectively. In Fig. 4(a) and 4(b), the horizontal direction is parallel to RD and vertical direction is parallel to TD. These typical in-plain domain patterns are usually called lancet domains and observed also by magnetic-optic Kerr microscopy in the previous study [39]. It demonstrates that Q<<1 also applies to $(Fe_{0.83}Ga_{0.17})_{99.8}Ag_{0.2}$ alloy. The domain arrangement is strongly dependent on the surface orientation relative to the easy magnetization directions [40]. The (110) surface only contains one easy magnetization axis (i.e., [001]), and lancet domains are often observed on slightly misoriented (110) surfaces. So, crystallographic orientation of observed areas in Fig. 4(a) and 4(b) are both slightly misoriented (110) surfaces, which are illustrated in Fig. 4(c). The flux is transported away from the surface, either to the opposite surface or towards the neighboring domains [37], which is shown in Fig. 4(d). The isolated lancets as well as the short kinks in the main walls in Fig. 4 (a) and 4(b) are connected with internal transverse domains [37]. The density of supplementary domains is related to the tilt misorientation θ of the grains. Domain width W and length L decrease inversely with increasing misorientation angle θ [39]. Thus, misorientation in $Fe_{0.83}Ga_{0.17}$ is larger

than that in $(Fe_{0.83}Ga_{0.17})_{99.8}Ag_{0.2}$, so transverse domain volume increases [41, 42]. The main contribution to dimension change comes from 90° domain rotation, and 180° domain wall motion has no effect on dimension change [11]. Thus, a larger volume of internal transverse domain induces larger magnetostriction when applied field is parallel to RD, i.e., $\lambda_{\parallel}$. This partly confirms that initial demagnetized state of $Fe_{0.83}Ga_{0.17}$ alloy is much closer than $(Fe_{0.83}Ga_{0.17})_{99.8}Ag_{0.2}$ alloy to ideal demagnetization from previous discussion. Since comparison of volume of internal transverse domains cannot be inferred from near (100) or (111) surfaces [37], those areas are not studied further. FeGa magnetic domain patterns in our study are analogous to Fe-3%Si investigated by MFM [43]. These domain patterns differ from maze-like domain patterns observed in FeGa polycrystals by MFM [44], and cellular domain structure in the arc-melted Fe-19%Ga polycrystal by the Bitter method [45].

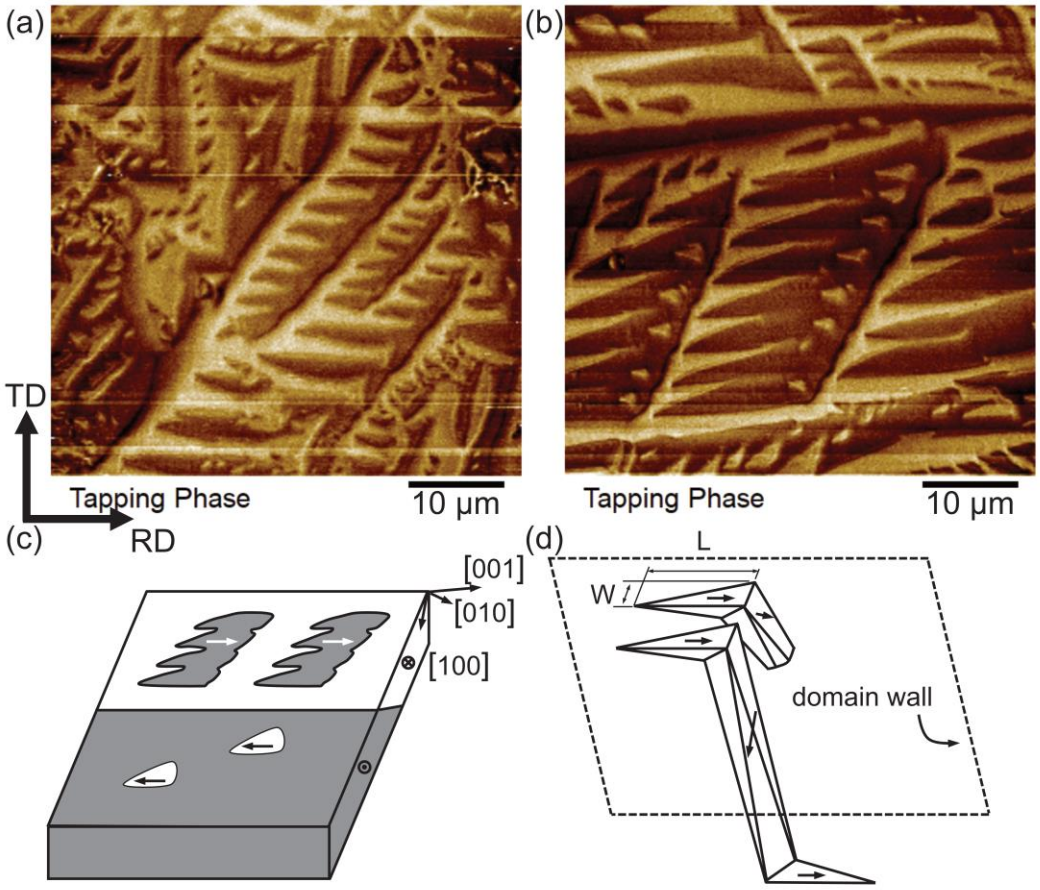

Fig. 4 Magnetic domain patterns of directionally solidified $(Fe_{0.83}Ga_{0.17})_{100-x}Ag_x$ samples in the slab plane at room temperature, (a) x=0, (b) x=0.2 by MFM. The horizontal direction is parallel to RD and vertical direction is

parallel to TD. (c) Internal domain structure. (d) illustrates that the flux is transported away from the surface, either to the opposite surface or towards the neighboring domains.

In summary, based on independence of $\lambda_s(=\ \lambda_{\parallel}-\lambda_{\perp})$ on magnetic domain distribution, a paradigm is proposed, combining ODF with magnetostriction tensor of single crystals. This paradigm not only quantifies the effects of texture on magnetostriction, but also accurately predicts λ_{100} in a trace amount of Ag-doped FeGa alloy. Given that ODFs and magnetostriction tensors of phases are obtained, based on the rule of mixture relationship, our paradigm can be extended to magnetostriction prediction in rare earth element-doped FeGa alloys and even other types of magnetostrictive materials. Our findings may accelerate the development of highly magnetostrictive alloys for sensor and actuator applications.

SUPPLEMENTARY MATERIAL

See supplementary material for the macrostructure investigated by optical microscopy.

Acknowledgment

This work was financially supported by the National Key R&D Program of China (2022YFE0109500, 2021YFB3501401), Natural Science Basic Research Program of Shaanxi (Program No. 2023-JC-ZD-24), the Space Science and Application Project of China Manned Space Engineering (Grant No. KJZ-YY-NCL10), the Key R&D Project of Shaanxi Province (2023GXLH-006), the Key R&D Project of Shaanxi Province (2022GXLH-01-07), Innovation Capability Support Program of Shaanxi (Nos. 2018PT-28, 2017KTPT-04), the Fundamental Research Funds for the Central Universities (China) and the World-Class Universities (Disciplines), the Characteristic Development Guidance Funds for the Central Universities (China).

The authors have no conflicts to disclose.

The data that support the findings of this study are available from the corresponding author upon reasonable request.

References

[1] KARACA H E, KARAMAN I, BASARAN B, et al. Magnetic field and stress induced martensite reorientation in NiMnGa ferromagnetic shape memory alloy single crystals [J]. Acta Mater, 2006, 54(1): 233-45.

[2] CLARK A E, SAVAGE H T. Magnetostriction of rare earth-Fe2 compounds under compressive stress [J]. J Magn Magn Mater, 1983, 31-34: 849–51.

[3] JIANG L, ZHANG G, YANG J, et al. Research on microstructure and magnetostriction of Fe83Ga17Dyx alloys [J]. J Rare Earths, 2010, 28: 409–12.

[4] JIANG L, YANG J, HAO H, et al. Giant enhancement in the magnetostrictive effect of FeGa alloys doped with low levels of terbium [J]. Appl Phys Lett, 2013, 102(22): 222409.

[5] LI J, XIAO X, YUAN C, et al. Effect of yttrium on the mechanical and magnetostrictive properties of $Fe_{83}Ga_{17}$ alloy [J]. J Rare Earths, 2015, 33(10): 1087–92.

[6] ZHAO X, TIAN X, YAO Z, et al. The origin of large magnetostrictive properties of rare earth doped Fe-Ga as-cast alloys [J]. J Magn Magn Mater, 2020, 514: 167289.

[7] MENG C Z, JIANG C B. Magnetostriction of a Fe83Ga17 single crystal slightly doped with Tb [J]. Scr Mater, 2016, 114: 9-12.

[8] ENGLER O, RANDLE V. Introduction to texture analysis: Macrotexture, microtexture, and orientation mapping [M]. 2nd ed. Boca Raton: CRC Press, 2010.

[9] BARUA R, TAHERI P, CHEN Y, et al. Giant Enhancement of Magnetostrictive Response in Directionally-Solidified $Fe_{83}Ga_{17}Er_x$ Compounds [J]. Materials, 2018, 11(6): 1039.

[10] ZHOU C, LIU Y, CHEN K, et al. Improved magnetostriction in Galfenol alloys by aligning crystal growth direction along easy magnetization axis [J]. Sci Rep, 2020, 10(1): 20055.

[11] HE Y, COEY J M D, SCHAEFER R, et al. Determination of bulk domain structure and magnetization processes in bcc ferromagnetic alloys: Analysis of magnetostriction in Fe83Ga17 [J]. Phys Rev Mater, 2018, 2(1): 014412.

[12] LI X, BAO X, LIU Y, et al. Tailoring magnetostriction with various directions for directional solidification Fe82Ga15Al3 alloy by magnetic field heat treatment [J]. Appl Phys Lett, 2017, 111(16): 162402.

[13] WU D, XING Q, MCCALLUM R W, et al. Magnetostriction of iron-germanium single crystals [J]. J Appl Phys, 2008, 103(7).

[14] WANG H, WU R. First-principles investigation of the effect of substitution and surface adsorption on the magnetostrictive performance of Fe-Ga alloys [J]. Phys Rev B, 2019, 99(20): 205125.

[15] WU Y, CHEN Y, MENG C, et al. Multiscale influence of trace Tb addition on the magnetostriction and ductility of ⟨100⟩ oriented directionally solidified Fe-Ga crystals [J]. Phys Rev Mater, 2019, 3(3): 033401.

[16] CAO K, DAI Z, ZHANG R, et al. Study on Magnetic Properties and the Nature of Phase Transition of Laves Phase Rare Earth-Transition Metal Compounds $Tb_{1-x}Dy_xCo_{1.95}$ [J]. Journal of Liaocheng University (Nat Sci Ed), 2024, 37(1): 29.

[17] HIELSCHER R, SCHAEBEN H. A novel pole figure inversion method: specification of the MTEX algorithm [J]. J Appl Crystallogr, 2008, 41(6): 1024–37.
[18] LEE M C, LIN C Y, WANG S H, et al. Soft-Magnetic Fe-Based Nano-Crystalline Thick Ribbons [J]. IEEE Trans Magn, 2008, 44(11): 3836-8.
[19] EVANS P G, DAPINO M J. Efficient model for field-induced magnetization and magnetostriction of Galfenol [J]. J Appl Phys, 2009, 105(11): 113901.
[20] LI J H, GAO X X, ZHU J, et al. Ductility, texture and large magnetostriction of Fe–Ga-based sheets [J]. Scr Mater, 2010, 63(2): 246–9.
[21] MAINPRICE D, HIELSCHER R, SCHAEBEN H. Calculating anisotropic physical properties from texture data using the MTEX open-source package [J]. Geol Soc Lond Spec Publ, 2011, 360(1): 175-92.
[22] SZPUNAR J A. Influence of crystal orientation distribution on anisotropy of magnetostriction and magnetocrystalline energy in Fe-Si steel [J]. J Appl Phys, 1984, 55(6): 2133-5.
[23] BUNGE H J. Texture and Magnetic Properties [J]. Textures Microstruct, 1989, 11: 727138.
[24] FEDERICO S, CONSOLO G, VALENTI G. Tensor representation of magnetostriction for all crystal classes [J]. Math Mech Solids, 2019, 24(9): 2814-43.
[25] CLARK A E, RESTORFF J B, WUN-FOGLE M, et al. Magnetostrictive properties of body-centered cubic Fe-Ga and Fe-Ga-Al alloys [J]. IEEE Trans Magn, 2000, 36(5): 3238–40.
[26] RAMíREZ G A, RIFFO A E M, GóMEZ J E, et al. Magnetoelasticity of $Fe_{1-x}Ga_x$ thin films on amorphous substrates [J]. Phys Rev B, 2021, 104(6): 064403.
[27] HE Y, JIANG C, WU W, et al. Giant heterogeneous magnetostriction in Fe–Ga alloys: Effect of trace element doping [J]. Acta Mater, 2016, 109: 177–86.
[28] CHEN Y, WANG J, YANG B, et al. Morphology evolution and enhanced magnetostriction of (Fe0.81Ga0.19)99.9Tb0.1 crystals prepared by liquid metal cooling Bridgman directional solidification [J]. J Alloys Compd, 2021, 856: 158166.
[29] YANG S, REN X. Noncubic crystallographic symmetry of a cubic ferromagnet: Simultaneous structural change at the ferromagnetic transition [J]. Phys Rev B, 2008, 77(1): 014407.
[30] LOGRASSO T A, ROSS A R, SCHLAGEL D L, et al. Structural transformations in quenched Fe–Ga alloys [J]. J Alloys Compd, 2003, 350(1): 95–101.
[31] ATULASIMHA J, FLATAU A B, SUMMERS E. Characterization and energy-based model of the magnetomechanical behavior of polycrystalline iron-gallium alloys [J]. Smart Mater Struct, 2007, 16(4): 1265-76.
[32] ZHAO L, TIAN X, YAO Z, et al. Enhanced magnetostrictive properties of lightly Pr doped Fe83Ga17 alloys [J]. J Rare Earths, 2019, 38(3): 257-64.
[33] WU W, LIU J, JIANG C, et al. Giant magnetostriction in Tb-doped $Fe_{83}Ga_{17}$ melt-spun ribbons [J]. Appl Phys Lett, 2013, 103(26): 262403.
[34] RAFIQUE S, CULLEN J R, WUTTIG M, et al. Magnetic anisotropy of FeGa alloys [J]. J Appl Phys, 2004, 95(11): 6939–41.
[35] RESTORFF J B, WUN-FOGLE M, CLARK A E, et al. Induced Magnetic Anisotropy in Stress-Annealed Galfenol Alloys [J]. IEEE Trans Magn, 2006, 42(10): 3087-9.
[36] MUDIVARTHI C. Magnetic and structural characterization of iron-gallium using Kerr microscopy and neutron scattering [D]; University of Maryland, College Park, 2010.
[37] HUBERT A, SCHäFER R. Magnetic domains: the analysis of magnetic microstructures [M]. Heidelberg: Springer, 1998.

[38] MUDIVARTHI C, NA S-M, SCHAEFER R, et al. Magnetic domain observations in Fe–Ga alloys [J]. J Magn Magn Mater, 2010, 322(14): 2023–6.
[39] SCHäFER R, SCHINNERLING S. Tomography of basic magnetic domain patterns in ironlike bulk material [J]. Phys Rev B, 2020, 101(21): 214430.
[40] BATISTA L, RABE U, HIRSEKORN S. Characterization of the magnetic micro- and nanostructure in unalloyed steels by magnetic force microscopy [J]. AIP Conf Proc, 2013, 1511(1): 1180-7.
[41] HE Z, SHA Y, ZHAO Z, et al. The calculation of magnetic domain and magnetostriction in stressed grain-oriented silicon steel [J]. J Appl Phys, 2020, 127(3).
[42] SHILLING J, HOUZE G. Magnetic properties and domain structure in grain-oriented 3% Si-Fe [J]. IEEE Trans Magn, 1974, 10(2): 195-223.
[43] SHIN S, SCHäFER R, COOMAN B C D. Grain Boundary Penetration by Lancet Domains in Fe-3%Si Grain-Oriented Steel [J]. IEEE Trans Magn, 2010, 46(9): 3574-81.
[44] ZHOU J K, LI D D, LI J G. Magnetic force microscopy observation of undercooled Fe81Ga19 magnetostrictive alloys [J]. J Phys D: Appl Phys, 2008, 41(20): 205405.
[45] TIANEN M N, SEGUIN D J, WANG Y U, et al. Cellular magnetic domains in Fe–Ga alloys [J]. Appl Phys Lett, 2020, 117(3): 032401.